Optica Applicata, Vol. XLIII, No. 4, 2013
DOI: 10.5277/oa130407

Fiber diameter influence on optical transport of dielectric particles along subwavelength optical fibers

YAO ZHANG, HONGXIANG LEI, BAOJUN LI*

State Key Laboratory of Optoelectronic Materials and Technologies,
School of Physics and Engineering, Sun Yat-Sen University,
Guangzhou 510275, China

*Corresponding author: stslbj@mail.sysu.edu.cn

We investigate a fiber diameter influence on optical transport of dielectric particles along subwavelength optical fibers using a near infrared laser of 1.55 μm wavelength. Theoretical analysis indicates that at 1.55 μm, the evanescent field at the fiber surface increases at first and then decreases with an increase of the fiber diameter from 600 nm to 1.6 μm, exhibiting a maximum at the fiber diameter of 950 nm. Based on three-dimensional finite-difference time-domain simulations, optical scattering forces acted on the dielectric particles and transport velocities of the particles were calculated for two fibers in the diameters of 930 nm and 1.5 μm. To support the theoretical analysis, experiments were performed using the two fibers to transport SiO_2 particles (sizes of 530 nm and 1.5 μm) and TiO_2 particles (size of 1.5 μm). The results show that with the same laser power launched into the two fibers, larger transport velocities can be obtained along the 930 nm diameter fiber.

Keywords: optical transport, optical scattering force, optical gradient force, subwavelength optical fiber, evanescent field.

1. Introduction

With a rapid progress in precise, contactless and non-destructive manipulation [1], optical force has become an extremely powerful tool for manipulating small particles or biological materials, especially in microfluidic platforms [2]. Among the manipulations of small objects in microfluidic platforms, transport along a predetermined direction is one of the key issues encountered in many research areas [3–6]. Particles suspended in liquids can be directly transported along the propagation direction of a single Gaussian or Bessel beam in free space systems [7–9]. Due to the considerable architecture volumes and the inconvenience in sample access, the free space system--based methods may face challenges in integration into opto-microfluidic platforms. To be easily incorporated into microfluidic systems, planar waveguides and optical

fibers have been employed to transport particles or cells through the evanescent field at the waveguide/fiber surfaces [10–21]. Compared with planar waveguides, optical fibers have a very low coupling loss and require no substrates, exhibiting flexibility in three-dimensional (3D) geometry. Therefore, optical fibers have become a preferable tool for particle transport in microfluidic platforms. Transport of polystyrene (PS) particles in water has been achieved by launching a 1.047 μm wavelength laser into a subwavelength optical fiber (950 nm diameter) [15], or by launching a 980 nm wavelength laser into a slightly tapered fiber (50 μm core diameter) [17]. The results show that the optical transport by using optical fibers is valid for a large range of fiber diameters. However, the transport performance is strongly related to the fiber diameter because the evanescent field at the fiber surface is mainly determined by the diameter [20, 21]. For a fixed laser wavelength, a proper fiber diameter can provide a stronger optical force and a faster transport for a particle. Therefore, in this work, an investigation of the fiber diameter influence on optical transport of dielectric particles is presented. Based on 3D finite-difference time-domain (FDTD) simulations, optical scattering forces acted on dielectric particles and the transport velocities of the particles were analyzed for fibers of different diameters at 1.55 μm wavelength. The theoretical results indicate that with the same optical power launched into the fibers, a larger transport velocity for the particle can be obtained along the fiber with the diameter of around 950 nm. By launching a 1.55- μm-wavelength laser into fibers in the diameters of 930 nm and 1.5 μm, optical transport was performed for SiO_2 particles (sizes of 530 nm and 1.5 μm) and TiO_2 particles (size of 1.5 μm). With the same laser power launched into the two fibers, the transport velocities of the particles along the 930 nm diameter fiber are larger than those along the 1.5 μm diameter fiber, which is consistent with the theoretical results.

2. Theoretical analysis

Figure 1 schematically shows the mechanism of optical transport of a particle along an optical fiber in water. As light propagates in the fiber, a portion of the light penetrates into water and forms evanescent field at the fiber surface. The evanescent field generates an optical gradient force F_g to trap the particle and an optical scattering force F_s to propel the particle along the propagation direction of the light. The magnitude of F_g and F_s is determined by the amplitude of the evanescent field which is strongly related to the fiber diameter. For relatively large diameters, the evanescent field at the fiber surface is small because most of light is confined within the fiber. With a decrease of the fiber diameter, the light gradually spreads into water and the evanescent field reaches a maximum. With a further decrease of the fiber diameter, a decay of the evanescent field occurs because most of light leaks out of the fiber. To numerically investigate the evanescent field at the surfaces of fibers with different diameters, 3D FDTD simulations were performed. In the simulations,

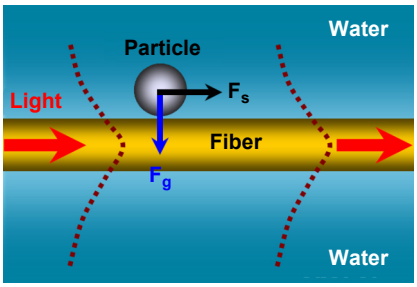

Fig. 1. Schematic of the mechanism of optical transport of a particle along an optical fiber in water. The dotted lines show the field intensity of the light inside and outside the fiber.

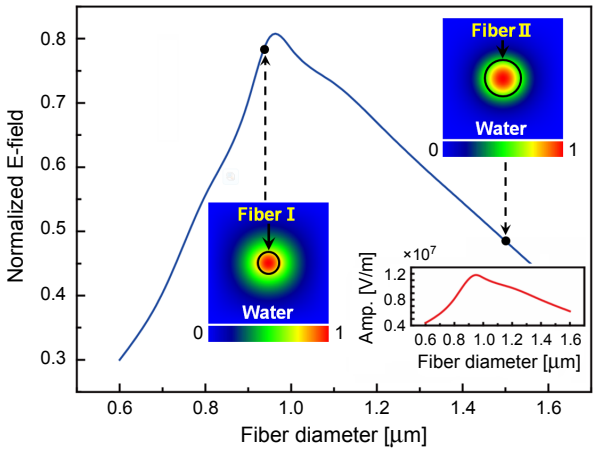

Fig. 2. Normalized electric-field (E-field) at the fiber surfaces as a function of the fiber diameter. The insets show the transversal cross-section views of the 3D FDTD simulated E-field distributions for two fibers in the diameters of 930 nm and 1.5 μm. The inset shows the true E-field amplitudes at the fiber surfaces (with an optical power of 1 W launched into the fibers).

the refractive indices of the fiber and the surrounding were set to be 1.45 and 1.33 for silica and water, respectively. The light wavelength launched into the fiber was set to be 1.55 μm. To cover the subwavelength range, the simulations were performed for the fibers with the diameters from 600 nm to 1.6 μm. In all simulations, the optical power launched into the fibers is set to be 1 W. Figure 2 shows the normalized electric--field (E-field) at the fiber surfaces as a function of the fiber diameter. The E-field at the surface was normalized to the maximum amplitude of the E-field inside the fibers obtained from the simulations. From Fig. 2, it can be seen that the normalized E-field reaches the maximum of 0.81 at the surface of a fiber with the diameter of 950 nm. Therefore, to obtain a strong evanescent field at the 1.55 μm wavelength, the fiber diameter should be close to 950 nm. For further analysis, two different fibers were

used for the following calculations. One has a diameter of 930 nm (fiber I), very close to 950 nm, and the other has a diameter of 1.5 μm (fiber II). The two fibers were also used for experiments, as to be presented in later sections. For 1.55 μm wavelength, the diameters of the both fibers are within the subwavelength range. The insets of Fig. 2 show the transversal cross-section views of the simulated E-field distributions on the two fibers. The normalized E-field at the surface of fiber I is 0.78, which is larger than that of fiber II (0.48). These indicate that with the same optical power, the evanescent field at the surface of fiber I is stronger than that of fiber II.

The total optical force F acted on a particle can be determined by [22]

$$F = \frac{n}{c}\iint \Delta S \, \mathrm{d}A \tag{1}$$

where n is the refractive index of the surrounding medium (water), c is the speed of light in vacuum, ΔS is the difference between the energy density flux traveling into and coming out of the unit area of the particle, and $\mathrm{d}A$ is the unit area of the particle. The force F consists of two orthogonal components, *i.e.*, the gradient force F_g and the scattering force F_s. So the F_g and F_s can be expressed as

$$F_g = \frac{n}{c}\iint \Delta S_{\perp} \, \mathrm{d}A \tag{2a}$$

$$F_s = \frac{n}{c}\iint \Delta S_{\parallel} \, \mathrm{d}A \tag{2b}$$

where $\Delta S_{\perp}$ is the component of ΔS perpendicular to the fiber and $\Delta S_{\parallel}$ is the component parallel to the fiber. To calculate F_g and F_s, simulations were performed for fibers I and II with a particle trapped near the fiber surface. For each of the two fibers, the simulations were repeated for a 530 nm diameter SiO_2 particle, a 1.5 μm diameter SiO_2 particle, and a 1.5 μm diameter TiO_2 particle. As the Debye length of the particle solutions used in later experiments is close to that reported in Ref. [23] (21 ± 9 nm), a gap of 30 nm is assumed between the particle and the fiber surface in the simulations. Also, the optical power of the 1.55 μm light launched into the fibers was set to be 1 W in all the simulations. Figure 3 shows the longitudinal views of the simulated energy density distributions of the fibers and the calculated F_g and F_s acted on the particle. For fiber I (Figs. 3**a**–3**c**), the calculated scattering forces F_s are 1.74, 8.08, and 21.02 pN acted on the 530 nm SiO_2 particle (Fig. 3**a**), 1.5 μm SiO_2 particle (Fig. 3**b**), and 1.5 μm TiO_2 particle (Fig. 3**c**). For fiber II (Figs. 3**d**–3**f**), the calculated scattering forces F_s are 0.67, 3.26, and 6.67 pN acted on the corresponding particles. The results indicate that with the same optical power launched into the two fibers, the scattering force F_s provided by fiber I is stronger than that provided by fiber II for the same particle.

As the scattering force propels the particle along the propagation direction of the light, the viscous drag force counteracts with the scattering force and limits

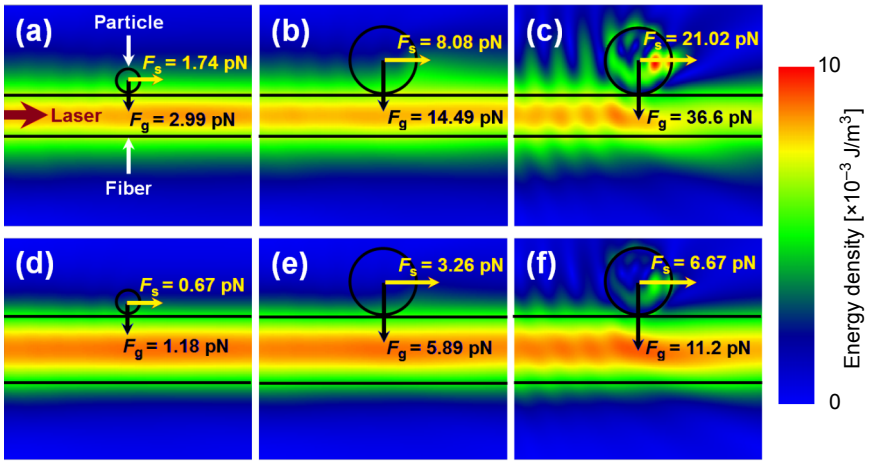

Fig. 3. Longitudinal views of the 3D FDTD simulated energy density distributions and the calculated F_g and F_s for fiber I (930 nm diameter) with (**a**) a 530 nm SiO_2 particle, (**b**) a 1.5 μm SiO_2 particle and (**c**) a 1.5 μm TiO_2 particle, and for fiber II (1.5 μm diameter) with (**d**) a 530 nm SiO_2 particle, (**e**) a 1.5 μm SiO_2 particle and (**f**) a 1.5 μm TiO_2 particle. Optical power of the 1.55 μm light launched into the fibers is 1 W.

the continuous acceleration of the particle, resulting in a terminal transport velocity. Generally, for a system exhibiting Stokesian drag, the transport velocity of the particle v_p can be determined by [14]

$$v_p = \frac{F_s}{C} \tag{3}$$

where C is a constant showing the relationship between the drag force and the transport velocity of the particle. In the case of a particle very close to the fiber surface, C can be expressed as

$$C = \frac{6\pi r\mu}{1 - \frac{9}{16}\left(\frac{r}{h}\right) + \frac{1}{8}\left(\frac{r}{h}\right)^3 - \frac{45}{256}\left(\frac{r}{h}\right)^4 - \frac{1}{16}\left(\frac{r}{h}\right)^5} \tag{4}$$

where r is the particle radius, μ is the dynamic viscosity of water, and h is the distance between the particle center and the fiber surface. Note that due to the low laser power (less than 100 mW) used in later experiments, the thermal effect is very limited [24] so it is assumed that there is no significant temperature change during the transport. Therefore, the room temperature dynamic viscosity of $\mu = 9.1\times10^{-4}$ Pa·s is used in the calculations. With Eqs. (3) and (4) and the calculated F_s, the transport velocity of the particle v_p was obtained (Table 1). All the results in Table 1 are obtained at the optical power of 1 W launched into the two fibers. It can be seen that for the same

T a b l e 1. Calculated optical scattering forces F_s and theoretical transport velocities of the particles along fibers I and II with optical power of 1 W launched into the two fibers.

	530 nm SiO_2 particle	1.5 μm SiO_2 particle	1.5 μm TiO_2 particle
F_s provided by fiber I	1.74 pN	8.08 pN	21.02 pN
F_s provided by fiber II	0.67 pN	3.26 pN	6.67 pN
Velocity along fiber I	165 μmm/s	231 μm/s	599 μm/s
Velocity along fiber II	64 μmm/s	93 μm/s	190 μm/s

optical power, the transport velocity along fiber I is higher than that along fiber II for the same particle. Note that since F_s is proportional to the energy flux through a particle, the transport velocity of the particle v_p at other optical powers can be directly obtained according to the results at 1 W listed in Table 1.

3. Experiments and results

To support the theoretical analysis, the experiments were performed using the two fibers to transport the three kinds of dielectric particles mentioned above. In the experimental setup (Fig. 4), a computer interfaced microscope with a CCD camera mounted on the top is used for real-time monitoring. To achieve fine positioning and mechanical stability, a slide (for holding the particle solution) is mounted on a translation stage for manipulation in *y*–*z* direction (50 nm resolution). A subwavelength optical fiber drawn from a commercial single-mode fiber by a flame-heating technique was laid above the slide, with its extremities held by two fiber positioners. Fibers I (930 nm diameter) and II (1.5 μm diameter) were drawn and used for the transport. The lengths of the subwavelength segments of fibers I and II are 210 μm and 190 μm, respectively. The length of the tapers at both sides of the two fibers is ~6 mm. The particle solutions were prepared by diluting the particles into water (volume ratio of particles to water

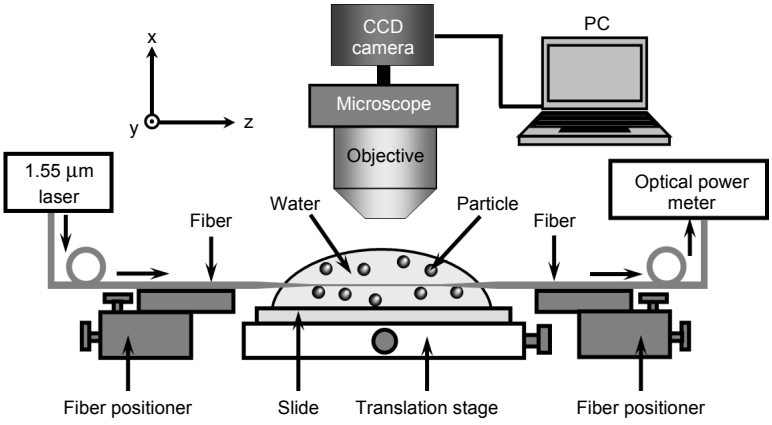

Fig. 4. Schematic of the experimental setup.

~1:1000) with the assistance of an ultrasonic shaker. The fiber was immersed in the particle solution, with one end connected to the 1.55 μm laser (variable power from 0 to 200 mW) and the other end connected to an optical power meter. The optical power meter was used to measure the output power from the fiber and thus estimate the optical power loss L before the launching into the subwavelength segment for each fiber. The loss L includes the coupling loss L_c from the laser to the fiber connector and the propagation loss L_p in the fiber taper before the subwavelength segment. To deduce L, at first, a single-mode fiber was directly connected to the 1.55 μm laser and the power meter for obtaining L_c. Then, the fiber after drawing was connected to the laser and the power meter again to obtain the total loss L_{total}. The total loss L_{total} consists of the coupling loss L_c and the propagation losses in the two fiber tapers before and after the subwavelength segments. Since the lengths of the two tapers are nearly the same (6 mm), the propagation loss L_p in one of the fiber tapers can be obtained by $L_p = (L_{\text{total}} - L_c)/2$. Therefore, the optical power loss L before launching into the subwavelength segment is $L = L_c + L_p$. In the experiments, the estimated values of L are 3 and 2.6 dB for fibers I and II, respectively. The output powers of the 1.55 μm laser were tuned according to the power loss L of the two fibers so that the same laser power launched into the two fibers was ensured. For each of the two fibers, optical transport was performed by using the three kinds of dielectric particles, *i.e.*, the 530 nm SiO_2 particles, 1.5 μm SiO_2 particles and 1.5 μm TiO_2 particles. The laser powers launched into the fibers were from 30 to 100 mW.

At first, optical transport of the particles along fiber I was performed. The laser power launched into fiber I was started with 30 mW. The solutions of the three kinds

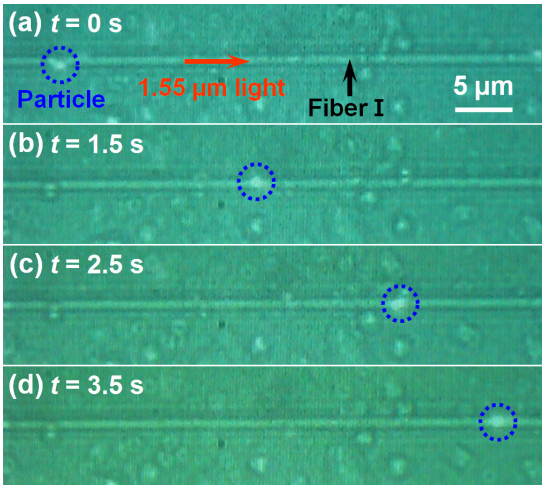

Fig. 5. Consecutive images captured by the CCD camera for the transport of a 530 nm SiO_2 particle along fiber I (930 nm diameter). The 1.55 μm laser power launched into the fiber was 90 mW. The transported particle is marked by a dashed circle. The time intervals between (**a**) and (**b**), (**b**) and (**c**), (**c**) and (**d**) are 1.5, 1, and 1 s, respectively.

of particles were individually used for measuring the transport velocity of the particles. For each kind of particles, measurements were taken for 10 particles to obtain the average transport velocity. The measurements were repeated for the transport at each laser power from 30 to 100 mW launched into the fiber. For illustration, Fig. 5 shows four consecutive images captured by the CCD camera for the transport of a 530 nm SiO_2 particle along fiber I when the 1.55 μm laser power launched into the fiber was 90 mW. The time intervals between Figs. 5**a** and 5**b**, 5**b** and 5**c**, and 5**c** and 5**d** are 1.5, 1, and 1 s, respectively. With the particle position in Fig. 5**a** as the reference point, the particle was transported 39 μm along fiber I in 3.5 s. So the transport velocity of this particle was ~11.1 μm/s. The average transport velocity for the 530 nm SiO_2 particles was 12.6 μm/s which was obtained from the measurements of 10 particles. The transport velocities for the 1.5 μm SiO_2 and TiO_2 particles at 90 mW and the velocities of the three kinds of particles at other laser powers (from 30 to 100 mW) were also obtained (presented in later sections). Then, the similar experiments and measurements were resumed by using fiber II. For illustration, Fig. 6 shows four consecutive optical microscope images for the transport of two 1.5 μm TiO_2 particles along fiber II when the 1.55 μm laser with power of 90 mW was launched into the fiber. The time interval in Fig. 6 is 1 s. With the positions of the two particles A

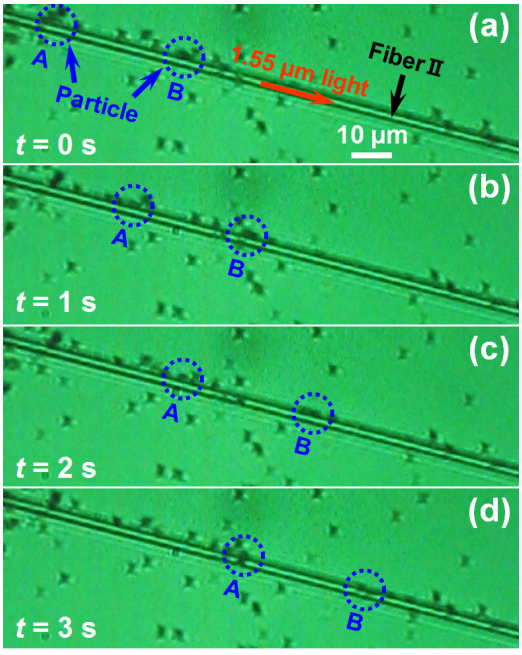

Fig. 6. Consecutive images captured by the CCD camera for the transport of two 1.5 μm TiO_2 particles along fiber II (1.5 μm diameter). The 1.55 μm laser power launched into the fiber was 90 mW. The two transported particles are marked by dashed circles and denoted by A and B. The time interval is 1 s.

and B in Fig. 6**a** as the respective reference points, the particles A and B were transported 49 and 50 μm, respectively, along fiber II in 3 s. So the transport velocities of A and B were ~16.3 and ~16.7 μm/s, respectively. Also, with the same method mentioned above, the average transport velocities of all the three kinds of particles along fiber II were obtained at other laser powers from 30 to 100 mW.

Figure 7 shows the measured transport velocities and the theoretically calculated results for the three kinds of particles along fibers I and II at different laser powers from 30 to 100 mW. Each point of the experimental data represents the average transport velocity of the measured 10 particles and the error bars represent standard deviation of velocity measurements for the given particles. Note that the experimentally measured transport velocities of the particles presented in Fig. 7 are consistently a little smaller than the theoretically calculated ones which are obtained from the optical scattering forces acting on a single particle. This difference can be explained

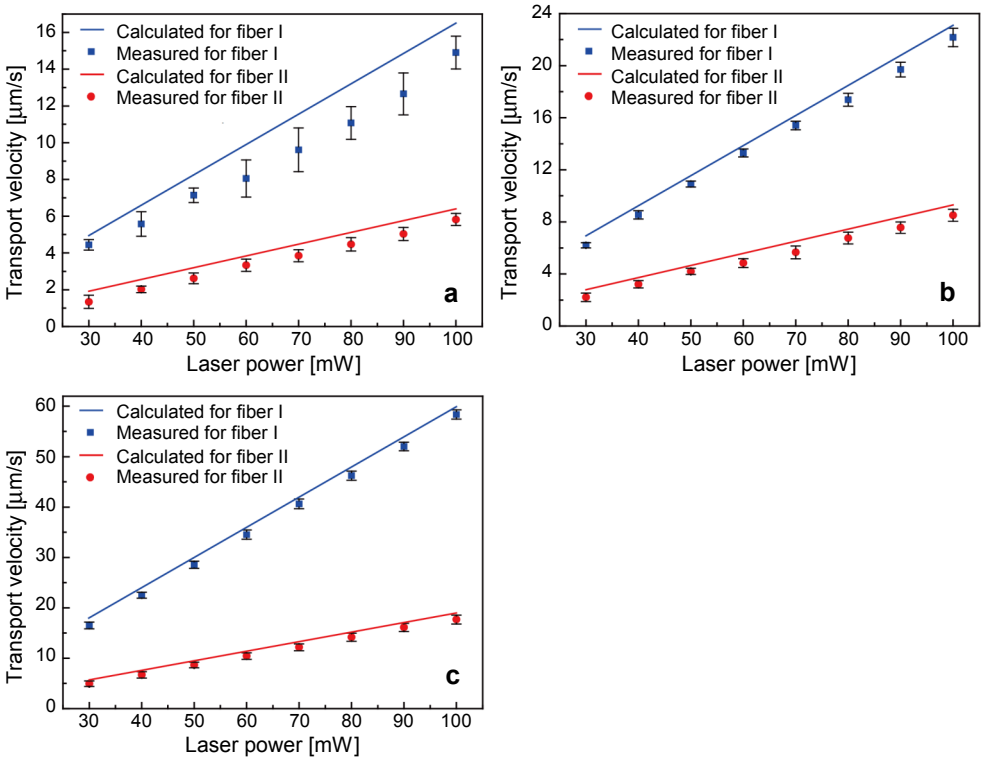

Fig. 7. Measured transport velocities and the theoretically calculated results for the (**a**) 530 nm SiO_2 particles, (**b**) 1.5 μm SiO_2 particles and (c) 1.5 μm TiO_2 particles along fibers I and II at different laser powers from 30 to 100 mW. Each point of the experimental data represents the average transport velocity of 10 particles. Error bars represent standard deviation of velocity measurements for the given particles.

as follows: *i*) since the particles are comparable in size to the fiber, the evanescent field distribution will be perturbed when multiple particles are simultaneously transported along the fiber. This leads to a more complicated evanescent field distribution and a modification of the optical forces. An investigation in Ref. [21] indicates that due to the evanescent field perturbation caused by the multiple particles, the magnitudes of the scattering forces exhibit a fluctuation. Moreover, due to the scattering and leakage effect caused by multiple particles, the scattering forces acting on these particles become smaller than those acting on the single particle. *ii*) With the increase in the laser power launched into the fiber, the optical gradient force will be gradually enhanced, which may lead to a decrease in the distance between the particles and the fiber surface. Thus the constant C in Eq. (3) will be increased and the velocities of the particles become smaller than the calculated ones. From Fig. 7**a**, it can be seen that for the 530 nm SiO_2 particles, the transport velocity increases with the laser power. This is in accordance with the theoretical results. Both the experimental and the theoretical results indicate that for the 530 nm SiO_2 particles, the transport velocity along fiber I is larger than that along fiber II. Similar results can also be found in Figs. 7**b** and 7**c** for the 1.5 μm SiO_2 and TiO_2 particles, respectively. These are also consistent with the theoretical results, confirming that with the same 1.55 μm laser power launched into the fibers, a larger transport velocity can be obtained along the fiber with the diameter closer to 950 nm. Therefore, for a given wavelength, the optical transport performance of a fiber can be optimized by choosing a proper fiber diameter that provides the strongest evanescent field at the fiber surface.

4. Conclusions

We theoretically and experimentally investigate the fiber diameter influence on optical transport of dielectric particles along subwavelength optical fibers using a near infrared laser. Based on 3D FDTD simulations, optical scattering forces and transport velocities were calculated for fibers with the diameters of 930 nm and 1.5 μm at the wavelength of 1.55 μm. Experiments were performed using the two fibers to transport 530 nm and 1.5 μm SiO_2 particles and 1.5 μm TiO_2 particles. Both the theoretical and the experimental results show that with the same 1.55 μm laser power launched into the two fibers, the transport velocities of the particles along the 930 nm diameter fiber are larger than those along the 1.5 μm diameter fiber. These results are expected to find applications in optimizing the optical transport performance of the optical fibers and be used for particle manipulation in microfluidic platforms.

Acknowledgements – The authors thank Professor Zhigang Cai from the School of Physics and Engineering, Sun Yat-Sen University for experimental assistance. This work was supported by the National Natural Science Foundation of China (Grants 61007038), China Postdoctoral Science Foundation (Grant 20100470952), and Guangdong Natural Science Foundation (Grant S2012010010061).

References

[1] GRIER D.G., *A revolution in optical manipulation*, Nature **424**(6950), 2003, pp. 810–816.

[2] HARDT S., SCHÖNFELD F., *Microfluidic Technologies for Miniaturized Analysis Systems*, Springer, New York, 2007.

[3] OZKAN M., WANG M., OZKAN C., FLYNN R., BIRKBECK A., ESENER S., *Optical manipulation of objects and biological cells in microfluidic devices*, Biomedical Microdevices **5**(1), 2003, pp. 61–67.

[4] WANG M.M., TU E., RAYMOND D.E., YANG J.M., ZHANG H., HAGEN N., DEES B., MERCER E.M., FORSTER A.H., KARIV I., MARCHAND P.J., BUTLER W.F., *Microfluidic sorting of mammalian cells by optical force switching*, Nature Biotechnology **23**(1), 2005, pp. 83–87.

[5] NAHMIAS Y., SCHWARTZ R.E., VERFAILLIE C.M., ODDE D., *Laser-guided direct writing for three-dimensional tissue engineering*, Biotechnology and Bioengineering **92**(2), 2005, pp. 129–136.

[6] ŠILER M., ČIŽMÁR T., JONÁŠ A., ZEMÁNEK P., *Surface delivery of a single nanoparticle under moving evanescent standing-wave illumination*, New Journal of Physics **10**(11), 2008, article 1130101.

[7] ASHKIN A., *Acceleration and trapping of particles by radiation pressure*, Physical Review Letters **24**(4), 1970, pp. 156–159.

[8] LITTLE H., BROWN C., GARCÉS-CHÁVEZ V., SIBBETT W., DHOLAKIA K., *Optical guiding of microscopic particles in femtosecond and continuous wave Bessel light beams*, Optics Express **12**(11), 2004, pp. 2560–2565.

[9] FISCHER P., CARRUTHERS A.E., VOLKE-SEPULVEDA K., WRIGHT E.M., BROWN C.T.A., SIBBETT W., DHOLAKIA K., *Enhanced optical guiding of colloidal particles using a supercontinuum light source*, Optics Express **14**(12), 2006, pp. 5792–5802.

[10] NG L.N., ZERVAS M.N., WILKINSON J.S., LUFF B.J., *Manipulation of colloidal gold nanoparticles in the evanescent field of a channel waveguide*, Applied Physics Letters **76**(15), 2000, pp. 1993–1995.

[11] TANAKA T., YAMAMOTO S., *Optically induced propulsion of small particles in an evenescent field of higher propagation mode in a multimode, channeled waveguide*, Applied Physics Letters **77**(20), 2000, pp. 3131–3133.

[12] GAUGIRAN S., GÉTIN S., FEDELI J.M., COLAS G., FUCHS A., CHATELAIN F., DÉROUARD J., *Optical manipulation of microparticles and cells on silicon nitride waveguides*, Optics Express **13**(18), 2005, pp. 6956–6963.

[13] GRUJIC K., HELLESO O.G., *Dielectric microsphere manipulation and chain assembly by counter--propagating waves in a channel waveguide*, Optics Express **15**(10), 2007, pp. 6470–6477.

[14] SCHMIDT B.S., YANG A.H.J., ERICKSON D., LIPSON M., *Optofluidic trapping and transport on solid core waveguides within a microfluidic device*, Optics Express **15**(22), 2007, pp. 14322–14334.

[15] BRAMBILLA G., MURUGAN G.S., WILKINSON J.S., RICHARDSON D.J., *Optical manipulation of microspheres along a subwavelength optical wire*, Optics Letters **32**(20), 2007, pp. 3041–3043.

[16] YANG A.H.J., MOORE S.D., SCHMIDT B.S., KLUG M., LIPSON M., ERICKSON D., *Optical manipulation of nanoparticles and biomolecules in sub-wavelength slot waveguides*, Nature **45**(7225), 2009, pp. 71–75.

[17] SHEU F.W., WU H.Y., CHEN S.H., *Using a slightly tapered optical fiber to attract and transport microparticles*, Optics Express **18**(6), 2010, pp. 5574–5579.

[18] AHLUWALIA B.S., MCCOURT P., HUSER T., HELLESO O.G., *Optical trapping and propulsion of red blood cells on waveguide surfaces*, Optics Express **18**(20), 2010, pp. 21053–21061.

[19] CAI H., POON A.W., *Optical manipulation and transport of microparticles on silicon nitride microring-resonator-based add-drop devices*, Optics Letters **35**(17), 2010, pp. 2855–2857.

[20] XU L., LI Y., LI B., *Size-dependent trapping and delivery of submicro-spheres using a submicrofibre*, New Journal of Physics **14**(3), 2012, article 033020.

[21] ZHANG Y., LI B., *Particle sorting using a subwavelength optical fiber*, Laser and Photonics Reviews **7**(2), 2013, pp. 289–296.

[22] ZHANG D., YUAN X.C., TJIN S.C., KRISHNAN S., *Rigorous time domain simulation of momentum transfer between light and microscopic particles in optical trapping*, Optics Express **12**(10), 2004, pp. 2220–2230.
[23] LIN S., SCHONBRUN E., CROZIER K., *Optical manipulation with planar silicon microring resonators*, Nano Letters **10**(7), 2010, pp. 2408–2411.
[24] ZHANG Y., LEI H., LI Y., LI B., *Microbe removal using a micrometer-sized optical fiber*, Lab on a Chip **12**(7), 2012, pp. 1302–1308.

Received February 6, 2013
in revised form April 5, 2013